Phase stability, elastic behavior, and pressure-induced structural evolution of kalsilite: A ceramic material and high-*T*/high-*P* mineral

G. Diego Gatta,[1,2,*] Ross J. Angel,[3] Jing Zhao,[3] Matteo Alvaro,[3] Nicola Rotiroti,[1,2] and Michael A. Carpenter[4]

[1]Dipartimento di Scienze della Terra, Università degli Studi di Milano, Via Botticelli 23, I-20133 Milano, Italy
[2]CNR Istituto per la dinamica dei processi ambientali, Via M. Bianco 9, I-20131 Milano, Italy
[3]Crystallography Laboratory, Department of Geosciences, Virginia Tech, Blacksburg, Virginia 24060, U.S.A.
[4]Department of Earth Sciences, University of Cambridge, Downing Street, Cambridge CB2 3EQ, U.K.

Abstract

The phase stability, elastic behavior, and pressure-induced structural evolution of a natural metamorphic kalsilite (ideal formula $KAlSiO_4$) from Punalur (Kerala district in southern India), with $P31c$ symmetry and a K/Na molar ratio of ~350, has been investigated by in situ X-ray single-crystal diffraction up to ~7 GPa with a diamond-anvil cell under hydrostatic conditions. At high-pressure, a previously unreported iso-symmetric first-order phase transition occurs at ~3.5 GPa. The volume compression of the two phases is described by third-order Birch-Murnaghan equations-of-state: V_0 = 201.02(1) Å^3, K_{T0} = 59.7(5) GPa, K' = 3.5(3) for the low-*P* polymorph, and V_0 = 200.1(13) Å^3, K_{T0} = 44(8) GPa, K' = 6.4(20) for the high-*P* polymorph. The pressure-induced structural evolution in kalsilite up to 7 GPa appears to be completely reversible. The compression of both phases involves tetrahedral rotations around [0001], which close up the channels within the framework. In addition, compression of the low-pressure phase involves tilting of the tetrahedra. The major structural change at the phase transition is an increase in the tilting of the tetrahedra, but with a reversion of the tetrahedral rotations to the value found at ambient conditions. This behavior is in distinct contrast to that of nepheline, which has a tetrahedral framework of the same topology.

Keywords: Crystal structure, kalsilite, XRD data, single crystal, high pressure, compressibility, structural evolution, compressibility measurements

Introduction

Kalsilite is a feldspathoid with ideal chemical formula: $KAlSiO_4$. In nature, kalsilite occurs mainly in K-rich and silica undersaturated volcanic rocks, usually associated with olivine, melilite, clinopyroxene, phlogopite, nepheline, and leucite. A few occurrences of methamorphic kalsilites have also been reported (e.g., Sandiford and Santosh 1991). Experiments on the stability of potassium aluminosilicates indicate that kalsilite is stable at least up to 15 GPa at 1300 K and, together with $KAlSi_3O_8$ (hollandite-type) and $K_2Si_4O_9$ (wadeite-type) phases, can be considered a potential host for K in anhydrous hyper-alkaline systems (Liu 1987).

In ceramic technology, kalsilite is used as the precursor for leucite, an important component in porcelain-fused-to-metal and ceramic restoration systems (Zhang et al. 2007). Kalsilite has also been proposed as a high thermal expansion ceramic for bonding to metals (Bogdanovicieni et al. 2008) and for the production of glass-ceramic seals for use in solid oxide fuel cells (Badding et al. 2009). Recently, nano-sized kalsilite has been demonstrated to show an excellent and highly improved oxidation activity of carbon toward diesel soot combustion (Kimura et al. 2008). Kalsilite is also used as a heterogeneous catalyst for *transesterification* (a process in which the organic group of an ester is exchanged with the organic group of an alcohol) of soybean oil with methanol to biodiesel (Wen et al. 2010).

The tetrahedral open-framework of kalsilite is isotypic with that of tridymite and nepheline, and has topological symmetry $P6_3/mmc$. The kalsilite framework consists of (0001) sheets of (ordered) AlO_4 and SiO_4 tetrahedra forming six-membered rings (hereafter 6mR), pointing alternately up (U) and down (D) [i.e., 6mR//(0001): UDUDUD, Fig. 1]. The sheets are stacked along the **c**-axis and are connected through the apical O1 atoms, which formally lie on special positions on the threefold axes. In volcanic Na-bearing kalsilites, this bridging oxygen may be displaced from the threefold axis (by up to ~0.25 Å), giving Al-O-Si bond angles <180° (Perrotta and Smith 1965). The tetrahedral 6mRs are also di-trigonally distorted by rotation of the tetrahedra around [0001], with the sense of rotation reversed between adjacent (0001) sheets in the $P6_3$ polymorph but with the same sense of rotation in all sheets of the $P31c$ polymorph that we have studied. A further set of 6mRs occurs perpendicular to (0001) [Fig. 1, hereafter 6mR⊥(0001)] that do not form channels.

Many experiments have been devoted to the phase stability, thermal behavior, and structural evolution at high- and low-temperature of kalsilite, which appear to be strongly controlled by the Na content (Tuttle and Smith 1958; Sahama 1962a, 1962b; Dollase and Freeborn 1977; Gregorkiewitz and Schäfer 1980; Andou and Kawahara 1982, 1984; Henderson and Taylor
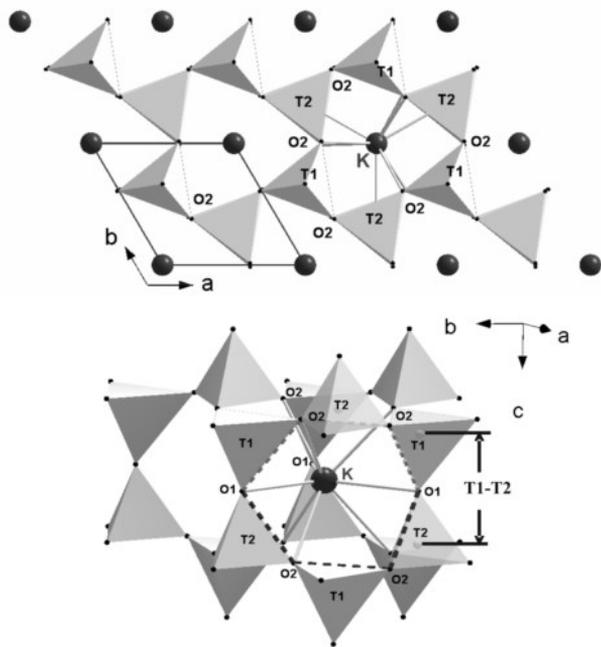
* E-mail: diego.gatta@unimi.it

FIGURE 1. Crystal structure of *P*31*c* kalsilite: (**top**) a single (0001) tetrahedral sheet of kalsilite, with 6mR//(0001), and (**bottom**) a clinographic view of the three-dimensional framework. The dark-gray and light-gray dotted lines outline the 6mR⊥(0001) indicate the O1-O2-O2′-O1′$_a$ and O1-O2-O2′-O1′$_b$ torsion angles, respectively (Table 4).

1982, 1988; Abbott 1984; Merlino 1984; Kawahara et al. 1987; Hovis and Roux 1993, 1999; Xu and Veblen 1996; Capobianco and Carpenter 1989; Carpenter and Cellai 1996; Fasshauer et al. 1998; Cellai et al. 1999; Hovis and Crelling 2000; Hovis et al. 2003, 2006, 2009; Gatta et al. 2010a). In particular, Cellai et al. (1997) reported the crystal structure of an essentially Na-free metamorphic kalsilite (i.e., K/Na molar ratio ~350) from Punalur (Kerala district in southern India). The authors showed that the structure has *P*31*c* symmetry at room conditions. The crystals were pervasively twinned across {0001}, so that *hkl* reflections of the first individual were superimposed on the *hkl̄* reflections of the second individual. The bridging oxygen between the sheets lies on the triad axis, giving an unusual Al-O-Si angle of 180°. No experimental evidence for splitting of the bridging oxygen off the threefold axis was reported, but a strong anisotropy of the thermal ellipsoid of the apical oxygen was observed, suggesting a static or dynamic disorder of the oxygen position and that the (apparent) inter-sheet Al-O-Si bond angle 180° is likely an artifact of averaging as found in some natural *P*6$_3$ kalsilites (e.g., Perrotta and Smith 1965). Carpenter and Cellai (1996) and Cellai et al. (1999) showed that the metamorphic *P*31*c* "pure" kalsilite experiences an "irreversible" phase transition to *P*6$_3$ upon heating to ~500 °C. The configuration of the high-temperature framework is achieved by tetrahedral rotation. The high-temperature structure shows strong similarities with that of the volcanic Na-bearing kalsilite at room conditions (i.e., with *P*6$_3$ symmetry at room conditions, Perrotta and Smith 1965). Recently, Gatta et al. (2010a) investigated the low-*T* behavior of the *P*31*c* kalsilite, using crystals of metamorphic kalsilite from the sample studied by Carpenter and Cellai (1996) and Cellai et al. (1997, 1999). Crystals of kalsilite that

were annealed at 900 °C for 1 h by Cellai and Carpenter (1999), and had previously exhibited *P*6$_3$ symmetry at room temperature, were selected. Surprisingly, all of the crystals checked by single-crystal X-ray diffraction showed *P*31*c* symmetry: the *P*31*c*-to-*P*6$_3$ phase transition upon heating reported as irreversible by Cellai et al. (1997) is actually reversible, on the timescale of a decade. Gatta et al. (2010a) described the thermo-elastic behavior at low *T* and suggested that the negative thermal expansion along [0001] observed between 100 and 300 K is a consequence of a decrease in the tetrahedral tilts with increasing temperature.

Despite the petrological importance of this mineral and technological uses of its synthetic counterpart, only one high-pressure experiment on this open-framework silicate has so far been reported. Fasshauer et al. (1998) measured the *P*-*V* equation of state of a synthetic *P*6$_3$ kalsilite up to 6.1 GPa by X-ray powder diffraction with a "quasi-hydrostatic" experiment conducted with a solid pressure medium. The elastic anisotropy is therefore unknown and the crystallographic characterization of the material at ambient conditions was performed only by the refinement of the unit-cell parameters on the basis of the powder diffraction pattern. On this basis, the aim of this study was the investigation of the phase stability, elastic behavior, and the pressure-induced structural evolution of a (Na-free) *P*31*c* kalsilite by means of in situ single-crystal X-ray diffraction with a diamond-anvil cell under hydrostatic conditions.

EXPERIMENTAL METHODS

The experiments in this study have been performed using a metamorphic kalsilite from the sample studied by Carpenter and Cellai (1996) and Cellai et al. (1997, 1999). The kalsilite crystals were collected from a granulite facies gneiss from Punalur, Kerala district, southern India, and provided by M. Santosh. In these rocks, kalsilite coexists with leucite, K-feldspar, hibonite, spinel, corundum, titanite, perovskite, and Ti-bearing phlogopite. Sandiford and Santosh (1991) estimated peak metamorphic conditions of the Punalur gneiss as 700–800 °C and 3.5–6.5 kbars. Kalsilite from Punalur is essentially end-member KAlSiO$_4$, with a K/Na molar ratio of ~350 (Capobianco and Carpenter 1989; Sandiford and Santosh 1991; Cellai et al. 1997, 1999).

A single crystal (130 × 110 × 40 μm³) of kalsilite was selected for the diffraction experiments. Precise and accurate unit-cell parameters were first measured with the crystal in air (Table 1) with a Huber four-circle diffractometer (non-monochromatized Mo*K*α radiation) using the eight-position centering protocol (King and Finger 1979; Angel et al. 2000; Angel and Finger 2011) of 28 Bragg reflections (Table 1). The lattice was found to be metrically trigonal, with unit-cell parameters of *a* = 5.1606(2) Å, *c* = 8.7164(1) Å, and *V* = 201.02(2) Å³. Intensity data were then collected on an Xcalibur-1 Oxford Diffraction diffractometer equipped with a CCD (Kappa-geometry, graphite-monochromatized Mo*K*α radiation) with the parameters reported in Table 2. No evidence of non-Bragg reflections was found. The crystal of kalsilite was found to be twinned by reticular merohedry with the {0001} twin plane, as previously observed for the Punalur kasilite (Cellai et al. 1997; Gatta et al. 2010a). The refined volumes of the two twin components approached 50% each. The reflection conditions were consistent with space group *P*31*c*, in agreement with Cellai et al. (1997, 1999) and Gatta et al. (2010a). Intensity data were then corrected for Lorentz-polarization (Lp) and absorption effects (analytical absorption correction by Gaussian integration based upon a physical description of the crystal) with the CrysAlis software (Oxford Diffraction 2009). The anisotropic structure refinement was performed with the SHELX-97 software (Sheldrick 2008), starting from the atomic coordinates of Gatta et al. (2010a), using neutral atomic scattering factors of K, Al, Si, and O from the *International Tables for Crystallography* (Wilson and Prince 1999). The refinement showed no threefold degeneracy of the oxygen O1 (Table 3[1]). The tetrahedral bond distances indicated

---

TABLE 1. Lattice parameters of kalsilite at pressure

P (GPa)	a (Å)	c (Å)	V (Å³)
0.0001*	5.1603(2)	8.7166(2)	201.01(2)
0.194(4)	5.1537(2)	8.7102(2)	200.36(1)
0.328(4)	5.1496(2)	8.7056(2)	199.93(2)
0.565(4)	5.1419(1)	8.6982(1)	199.17(1)
1.184(4)	5.1229(1)	8.6765(1)	197.20(1)
1.514(6)	5.1130(1)	8.6646(1)	196.17(1)
2.014(4)	5.0992(2)	8.6459(2)	194.69(1)
2.392(5)	5.0895(2)	8.6310(2)	193.61(1)
2.624(6)	5.0840(2)	8.6213(2)	192.98(1)
3.047(5)	5.0753(6)	8.5956(6)	191.75(5)
3.251(5)	5.0712(7)	8.5853(7)	191.21(5)
3.529(6)	5.0657(9)	8.5703(10)	190.46(7)
3.942(8)	5.0711(2)	8.3742(3)	186.50(2)
4.057(8)	5.0678(2)	8.3684(2)	186.13(2)
4.510(8)	5.0572(2)	8.3482(2)	184.90(1)
4.996(8)	5.0469(2)	8.3280(2)	183.71(1)
5.507(9)	5.0367(1)	8.3080(2)	182.53(1)
6.060(9)	5.0256(2)	8.2855(2)	181.23(1)
6.478(8)	5.0167(2)	8.2693(2)	180.23(1)
6.860(9)	5.0101(3)	8.2559(3)	179.47(2)
5.174(6)†	5.0435(2)	8.3205(2)	183.29(1)
4.351(8)†	5.0615(2)	8.3541(2)	185.34(1)
4.006(6)†	5.0690(2)	8.3679(2)	186.20(1)
3.808(8)†	5.0743(3)	8.3786(3)	186.83(3)
3.600(6)†	5.0788(2)	8.3884(3)	187.39(2)
3.583(6)†	5.0788(2)	8.3890(2)	187.40(2)
3.453(7)†	5.0695(13)	8.5753(13)	190.85(10)

Note: Lattice parameters with the crystal in air are: $a = 5.1606(2)$, $c = 8.7164(1)$ Å and $V = 201.02(2)$ Å³. Estimated standard deviations in the last digit are in parentheses.
* Crystal in the DAC without *P*-medium.
† In decompression.

an essentially complete Si/Al-ordering (Table 4). The refined site occupancy of the extra-framework K-site was found to be slightly lower than 100% (Table 3[1]). No peak larger than $\pm 0.8 e^-/Å^3$ was present in the final difference Fourier synthesis at the end of the refinement. Further details of the structure refinement are reported in Tables 2, 3[1], and 4.

An ETH-type diamond-anvil cell (DAC), as described by Miletich et al. (2000), was used for the high-pressure experiments. A 250 μm thick T301 steel foil was used as a gasket. It was pre-indented to a thickness of about 110 μm before drilling a hole (⌀ 300 μm) by spark-erosion. The same crystal of kalsilite previously investigated at ambient conditions was placed into the gasket hole together with some ruby chips and a single-crystal of quartz used for pressure measurement (Mao et al. 1986; Angel et al. 1997). A 4:1 mixture of methanol:ethanol was used as the hydrostatic pressure-transmitting medium (Angel et al. 2007). Lattice parameters were measured between 0.0001 and 6.860(9) GPa (Table 1), using 21 Bragg reflections and the same peak-centering protocol adopted for the crystal in air. Nine full data collections at pressures 0.0001 GPa (with crystal in DAC without any pressure medium), 0.90(5), 1.33(10), 2.30(10), 3.05(10), 3.27(10), 4.62(11), 4.94(10) and 6.24(9) GPa were performed with an Xcalibur-1 Oxford Diffraction diffractometer equipped with a CCD (Kappa-geometry, graphite-monochromatised Mo*K*α radiation). No violation of the reflection conditions expected for the space group *P*31*c* were observed at any pressure. Integrated intensity data were corrected for Lp and absorption effects due to the crystal and the DAC using the ABSORB computer program (Burnham 1966; Angel 2004). Anisotropic displacement parameters were refined only for the extra-framework site. Atomic coordinates and displacement parameters are listed in Table 3[1], and bond distances and angles in Table 4. CIFs are deposited[1]. The unit-cell parameters measured in decompression showed that the pressure-induced structural evolution up to 6.9 GPa is completely reversible.

RESULTS

Unit-cell parameters and elasticity

The evolution of the unit-cell parameters of kalsilite up to about 6.9 GPa is shown in Figure 2. It is clear from these data, and especially from the evolution of the *c/a* ratio with *P* (Fig. 2), that there are three distinct regimes in the compressional behavior of kalsilite as well as a first-order phase transition. Between 0.0001 and ~2–2.5 GPa, a "normal" compressional behavior is observed, with a positive monotonic trend of the *c/a* ratio with pressure. Above 2.0 GPa, there is a stiffening of the *a*-axis, and between ~2.5 and ~3.5 GPa a pronounced softening of the *c*-axis leading to a decrease in the *c/a* ratio with *P*. In this last pressure range, all of the Bragg reflections except the 00*l* reflections show significant broadening, and this resulted in a significant increase of the e.s.d. values of the unit-cell parameters

TABLE 2. Details of data collection and refinements of kalsilite at different pressures

P (GPa)	0.0001	0.0001*	0.90(5)	1.33(10)	2.30(10)	3.05(10)	3.27(10)	4.62(11)	4.94(10)	6.24(9)
a (Å)	5.1552(16)	5.169(1)	5.138(2)	5.125(3)	5.099(3)	5.081(3)	5.079(4)	5.061(5)	5.048(3)	5.024(2)
c (Å)	8.7096(19)	8.714(2)	8.691(3)	8.676(6)	8.637(6)	8.605(4)	8.587(5)	8.315(9)	8.322(6)	8.261(3)
V (Å³)	200.46(10)	201.66(9)	198.7(1)	197.4(2)	194.5(5)	192.4(2)	191.8(2)	184.4(3)	183.7(2)	180.6(1)
Space group	P31c	P31c	P31c	P31c	P31c	P31c	P31c	P31c	P31c	P31c
θ max (°)	36.01	40.62	40.89	40.48	40.52	40.69	38.91	40.54	40.67	40.56
No. measured reflections	5686	1482	1410	1340	1369	1320	1228	1205	1206	1131
No. unique reflections	626	582	553	532	525	508	448	461	457	426
No. unique reflections with $F_o > 4\sigma(F_o)$	473	244	227	216	217	215	184	178	171	158
No. refined parameters	24	16	16	16	16	16	16	15	15	15
R_{int}	0.0425	0.0810	0.1028	0.0877	0.1286	0.1339	0.1451	0.1384	0.1349	0.1455
R_1 (F) with $F_o > 4\sigma(F_o)$	0.0371	0.0632	0.0691	0.0621	0.0918	0.1078	0.1312	0.1188	0.1185	0.1171
$wR_2(F^2)$	0.0730	0.1305	0.1407	0.1178	0.1282	0.1379	0.1458	0.1440	0.1586	0.1353
GooF	1.511	1.062	1.166	1.081	1.093	1.043	1.230	1.736	1.849	1.630
Residuals ($e^-/Å^3$)	−0.63±0.79	−0.97±0.91	−1.13±1.14	−1.22±0.98	−0.89±0.80	−1.09±0.72	−1.04±1.01	−1.39+1.27	−1.41±1.29	−1.69±1.19

P (GPa)	4.62(11)†	4.94(10)†	6.24(9)†
No. refined parameters	17	17	17
R_{int}	0.1384	0.1349	0.1455
R_1 (F) with $F_o > 4\sigma(F_o)$	0.1153	0.1166	0.1107
$wR_2(F^2)$	0.1379	0.1527	0.1285
GooF	1.614	1.745	1.510
Residuals ($e^-/Å^3$)	−1.02/+1.17	−1.08/+1.36	−1.09/+1.20

Notes: For all of the data collections: Mo*K*α radiation, CCD detector type, ω/φ scan type, 60 s of exposure time per frame. The crystal of kalsilite was twinned by reticular merohedry with the {0001} twin plane, and the refined volumes of the two twin components approached 50% each at all pressures. The Flack parameter (Sheldrick 1997) is approximately $x = 0.5$ at any pressure. At 4.62, 4.94, and 6.24 GPa, a full K site occupancy was obtained within the e.s.d. values; therefore, it was fixed. Estimated standard deviations are in parentheses. $R_{int} = \Sigma|F_{obs}^2 - F_{obs}^2(mean)|/\Sigma[F_{obs}^2]$; $R_1 = \Sigma(|F_{obs}| - |F_{calc}|)/\Sigma|F_{obs}|$; $wR_2 = \{\Sigma[w(F_{obs}^2 - F_{calc}^2)^2]/\Sigma[w(F_{obs}^2)^2]\}^{0.5}$, $w = 1/[\sigma^2(F_{obs}^2) + (0.01*P)^2]$, $P = [Max(F_{obs}^2,0) + 2*F_{calc}^2]/3$.
* With the crystal in the DAC without any *P*-medium.
† Refinements with the O1 split-site model.

TABLE 4. Selected bond distances (Å) and angles (°) and other structural parameters of kalsilite at different pressures

P (GPa)	0.0001	0.0001*	0.90(5)	1.33(10)	2.30(10)	3.05(10)	3.27(10)	4.62(11)	4.94(10)	6.24(9)
K-O2 (×3)	2.958(8)	2.956(15)	2.926(15)	2.876(13)	2.864(19)	2.831(12)	2.863(16)	2.683(7)	2.697(8)	2.674(9)
K-O2′(×3)	2.975(8)	2.986(16)	2.967(16)	2.984(13)	2.955(19)	2.980(13)	2.938(18)	3.097(9)	3.040(11)	3.020(12)
K-O1 (×3)	2.977(1)	2.9851(8)	2.967(1)	2.959(2)	2.944(2)	2.934(2)	2.933(2)	2.924(3)	2.917(2)	2.905(1)
<K-O>	2.970	2.973	2.953	2.940	2.921	2.915	2.908	2.901	2.885	2.866
T1-O1	1.715(4)	1.710 (7)	1.707(7)	1.705(7)	1.694(7)	1.693(7)	1.694(7)	1.650(6)	1.658(6)	1.656(6)
T1-O2 (×3)	1.731(3)	1.731(4)	1.728(4)	1.729(4)	1.722(8)	1.711(7)	1.718(8)	1.701(5)	1.688(5)	1.676(5)
<T1-O>	1.727	1.725	1.723	1.723	1.715	1.706	1.712	1.688	1.681	1.671
O1-T1-O2 (×3)	106.6(3)	106.9(7)	106.2(7)	109.7(6)	109.0(9)	104.2(5)	104.6(7)	98.7(3)	100.5(4)	101.1(4)
O2-T1-O2 (×3)	112.2(3)	111.9(6)	112.5(6)	109.3(6)	109.9(9)	114.2(4)	113.9(6)	117.7(2)	116.7(2)	116.4(3)
T2-O1	1.611(4)	1.611(7)	1.607(7)	1.602(7)	1.599(7)	1.598(7)	1.597(8)	1.559(6)	1.567(6)	1.566(6)
T2-O2 (×3)	1.616(3)	1.626(4)	1.623(4)	1.623(4)	1.620(8)	1.616(8)	1.605(8)	1.591(6)	1.592(7)	1.579(7)
<T2-O>	1.615	1.622	1.619	1.618	1.614	1.611	1.602	1.583	1.586	1.576
O1-T2-O2 (×3)	109.3(4)	109.1(7)	109.7(7)	106.1(7)	106.6(9)	111.5(6)	110.8(8)	115.7(4)	113.2(5)	111.8(5)
O2-T2-O2 (×3)	109.6(4)	109.8(7)	109.2(7)	112.7(6)	112.2(8)	107.4(6)	108.1(8)	102.5(5)	105.5(5)	107.1(5)
T1-T2	3.326(4)	3.321(7)	3.314(7)	3.307(7)	3.293(7)	3.291(7)	3.291(7)	3.209(6)	3.225(6)	3.222(6)
O2-O2-O2$_s$[6mR//(0001)]	78.4(1)	78.4(2)	77.2(2)	76.3(2)	75.5(3)	76.0(2)	75.9(3)	79.3(2)	77.9(2)	77.5(2)
O2-O2-O2$_i$[6mR//(0001)]	161.6(2)	161.6(3)	162.9(3)	163.8(3)	164.5(4)	164.0(3)	164.1(4)	160.7(2)	162.1(3)	162.5(3)
O2-O1-O2 [6mR⊥(0001)]	107.7(3)	107.6(4)	107.5(4)	107.3(5)	107.2(6)	107.4(4)	107.3(6)	106.1(3)	106.2(3)	106.0(3)
O2-O2-O1	124.6(2)	124.8(3)	124.3(3)	126.0(3)	125.6(4)	123.3(3)	123.5(4)	121.9(2)	122.8(3)	123.3(3)
O1-O2-O2′-O1′$_a$	42.1(4)	42.5(7)	43.1(7)	46.3(7)	46.6(9)	42.8(6)	43.2(9)	37.7(4)	40.3(5)	41.4(5)
O1-O2-O2′-O1′$_b$	44.1(4)	43.9(7)	45.2(7)	44.0(6)	45.0(9)	47.8(7)	47.7(9)	49.0(5)	48.8(5)	48.6(6)

P (GPa)	4.62(11)†	4.94(10)†	6.24(9)†
K-O2 (×3)	2.685(7)	2.692(8)	2.677(8)
K-O2′ (×3)	3.095(9)	3.06(1)	3.02(1)
K-O1 (×3)	2.63(1)	2.62(2)	2.54(1)
K-O1′(×3)	2.91(1)	2.91(3)	2.98(2)
K-O1″(×3)	3.275(6)	3.27(1)	3.23(1)
T1-O1 (×3)	1.686(6)	1.694(6)	1.690(6)
T1-O2 (×3)	1.707(5)	1.697(5)	1.684(5)
<T1-O>	1.697	1.696	1.687
T2-O1 (×3)	1.593(6)	1.600(6)	1.600(6)
T2-O2 (×3)	1.591(6)	1.590(7)	1.581(7)
<T2-O>	1.592	1.595	1.591
T1-O1-T2	153.2(4)	153.3(5)	152.2(4)
T1-T2	3.190(6)	3.205(6)	3.193(5)
O2-O2-O2$_s$[6mR//(0001)]	79.3(2)	78.2(2)	77.6(2)
O2-O2-O2$_i$[6mR//(0001)]	160.7(2)	161.8(2)	162.4(4)

Notes: Estimated standard deviations are in parentheses. The torsion angles O1-O2-O2′-O1′$_a$ and O1-O2-O2′-O1′$_b$ are defined according to Klyne and Prelog (1960).
* With the crystal in the DAC without any *P*-medium.
† Refinements with the O1 split-site model.

(Table 1). This regime appears to be the precursor to a first-order phase transition just above 3.5 GPa that has never been previously reported in the literature. The transition pressure was bracketed between 3.529(8) and 3.600(6) GPa by several reversal measurements in compression and decompression, and we were unable to demonstrate a hysteresis. The phase transition on increasing pressure gives rise to an expansion of the structure on (0001) and to a strong compression along [0001] (Fig. 2) that combine to produce a ~0.4% volume decrease. Optical and diffraction observations show that the phase transition does not lead to a further twinning of the crystal. Above the transition, the Bragg diffraction peaks become sharp again, with the same widths as measured below 2.6 GPa. The HP-polymorph has a metrically trigonal lattice, and the evolution of its unit-cell parameters with *P* is continuous and monotonic up to 6.9 GPa, without any evidence of a further phase transition or anomalous elastic behavior within the *P*-range investigated.

The variation of the volume of the low-*P* polymorph shows no evidence in the *fe-Fe* plot (Fig. 3) of the changes seen in the evolution of the individual cell parameters, and can therefore be described by a single third-order Birch-Murnaghan equation-of-state (Birch 1947) with $V_0 = 201.02(1)$ Å³, $K_{T0} = 59.7(5)$ GPa, $K' = 3.5(3)$. The same equation fit to the *P-V* data for the high-pressure polymorph shows that it is significantly softer than the

low-pressure polymorph at the pressure of the phase transition, and also if the bulk moduli are compared at room pressure: $V_0 = 200.1(13)$ Å³, $K_{T0} = 44(8)$ GPa, $K' = 6.4(20)$.

The *fe-Fe* plots (Fig. 3) show that the variation of both unit-cell parameters of the high-pressure polymorph can be described in terms of a second-order linearized BM EoS (Angel 2000) with $K' = 4$. Weighted fits give: $a_0 = 5.170(1)$ Å and $K_{T0}(a) = 59.8(6)$ GPa for the *a*-axis and $c_0 = 8.575(1)$ Å and $K_{T0}(c) = 47.8(3)$ GPa for the *c*-axis, showing that the (0001) or *a-b* plane is about 25% stiffer in compression than the perpendicular [0001] axis. The behavior of the unit-cell parameters of the low-pressure polymorph is much more complex (Fig. 3), and neither can be described by a single equation of state. We therefore fit the data only up to pressures at which significant abnormal compression occurs, purely to obtain a reasonable estimate of the low-pressure compressional moduli. The refined elastic parameters for the low-*P* polymorph are: $a_0 = 5.1602(1)$ Å and $K_{T0}(a) = 52.0(3)$ GPa with K' fixed to 4 for the *a*-axis data up to 1.6 GPa, and $c_0 = 8.7166(2)$ Å and $K_{T0}(c) = 89.7(7)$ GPa and $K' = -6.2(4)$ for the *c*-axis up to 2.62 GPa. The elastic anisotropy of the low-pressure phase with the [0001] axis being stiffer than the (0001) plane is the reverse of that in the high-pressure phase. Note the strongly negative value for K' of the *c*-axis that indicates that elastic softening occurs prior to the phase transition.
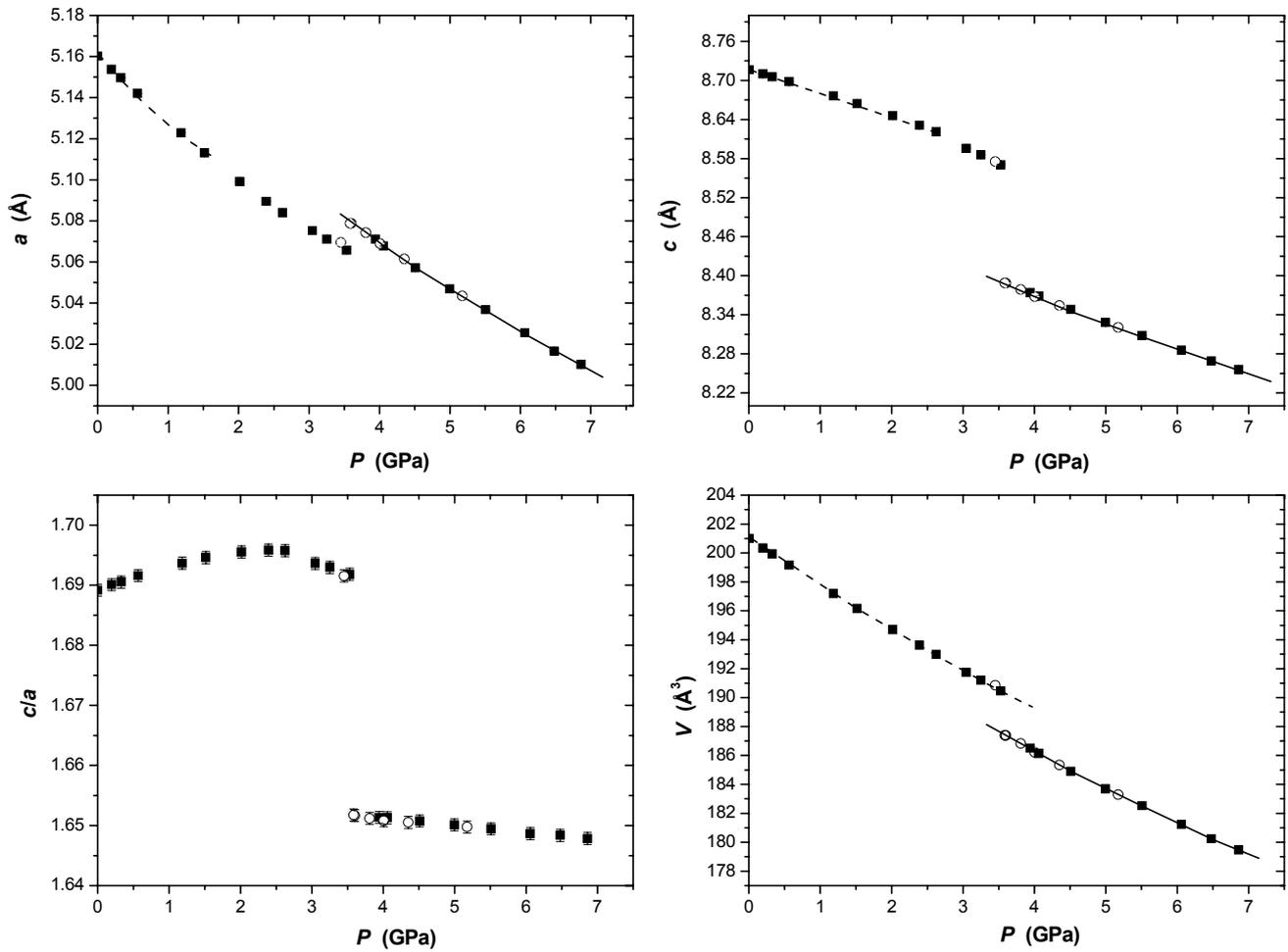
FIGURE 2. Variation of the unit-cell parameters of kalsilite with pressure. Open symbols represent data collected in decompression. The dashed and solid lines represent the axial and volume third-order Birch-Murnaghan EoS fits for the low-*P* and high-*P* polymorphs, respectively. The e.s.d. values are slightly smaller than the size of the symbols.

Structural evolution with pressure: tetrahedral framework

Within the average structure of *P*31*c* kalsilite at room conditions, the tetrahedral T1 and T2 sites and the bridging O1 oxygen lie on the triad axis (at $x = 1/3$, $y = 2/3$), which makes the T1-O1-T2 linkage linear. Therefore, if the kalsilite structure conforms strictly to the global *P*31*c* symmetry, the only degrees of freedom available to accommodate compression are tetrahedral compression and deformation of the O-T-O bond angles, and the rotation of the tetrahedra around [0001]. To describe the rotations, we define a rotation angle "δ" that describes the rotation of the tetrahedra from the un-rotated state they would have in the (hypothetical) structure with the topochemical symmetry *P*6₃*mc* (Gottardi 1979; Fig. 4a). Because all of the O2 atoms in one layer of tetrahedra have the same *z*-coordinate by symmetry in both *P*31*c* and *P*6₃*mc*, the O2-O2-O2 angles can be used to define the tetrahedral rotation as $\delta = |120 - (O2\text{-}O2\text{-}O2)|/2$ (Fig. 4b). When the tetrahedra are not rotated, the O2-O2-O2 angles are all 120°. Rotation reduces and increases adjacent O2-O2-O2 angles by the same amount, so that two adjacent angles in the ring always sum to 240°. Using the absolute value in the numerator in the expression for δ ensures that the same value is obtained whichever of the two O2-O2-O2 angles is used. The maximum

possible rotation of δ = 30° corresponds to O2-O2-O2 angles of 60° and 180°. In kalsilite at room conditions, the O2-O2-O2 angles are 78.4° and 161.6°, so the rotation angle δ is 20.8°. The projected triangle T1-O2-T2 (Fig. 4b) also provides the relationship between the length of the cell edge, *a*, and the rotation angle as $a/\sqrt{3} = 2l\cos\delta$, where *l* is the average of the lengths of the T1-O2 and T2-O2 bonds projected on to the (0001) plane. Thus, if the tetrahedra are rigid, rotations increase δ and reduce the *a* unit-cell parameter.

There is strong evidence that in the local structure of kalsilite the tetrahedra are tilted in addition to being rotated. The T1-T2 distance across the O1 oxygen of ~3.32 Å is too short at room conditions to accommodate normal values for Al-O and Si-O bonds. The large values of the thermal displacement parameter U_{11} for the O1 oxygen suggest static or dynamic displacements from the triad at $x = 1/3$, $y = 2/3$. The large value at room conditions of U_{33} for the O2 basal oxygen of the tetrahedra (Table 3[1]) suggests that the O1 displacement is due to local tilting of the tetrahedra that locally breaks the *P*31*c* symmetry (e.g., Gatta et al. 2010a). The tilting in kalsilite is not as large at room conditions as the one observed in nepheline, and it is not possible to refine a split-site model for the O1 position for kalsilite. The O1 site

FIGURE 3. Volume and axial Eulerian finite strain vs. normalized stress (*fe-Fe* plot) for kalsilite; e.s.d. values calculated according to Heinz and Jeanloz (1984) and Angel (2000), including the measured uncertainty in V_0, a_0, and c_0. The dashed and solid lines represent the weighted linear regressions through the data points for the low-*P* and high-*P* polymorphs, respectively, and the refined *Fe*(0) and *K'* values are reported. For the high-*P* polymorph, strain, and stress were calculated using the a_0, c_0, and V_0 values refined with a Birch-Murnaghan EoS fit, and the error bars include the uncertainties in these values.
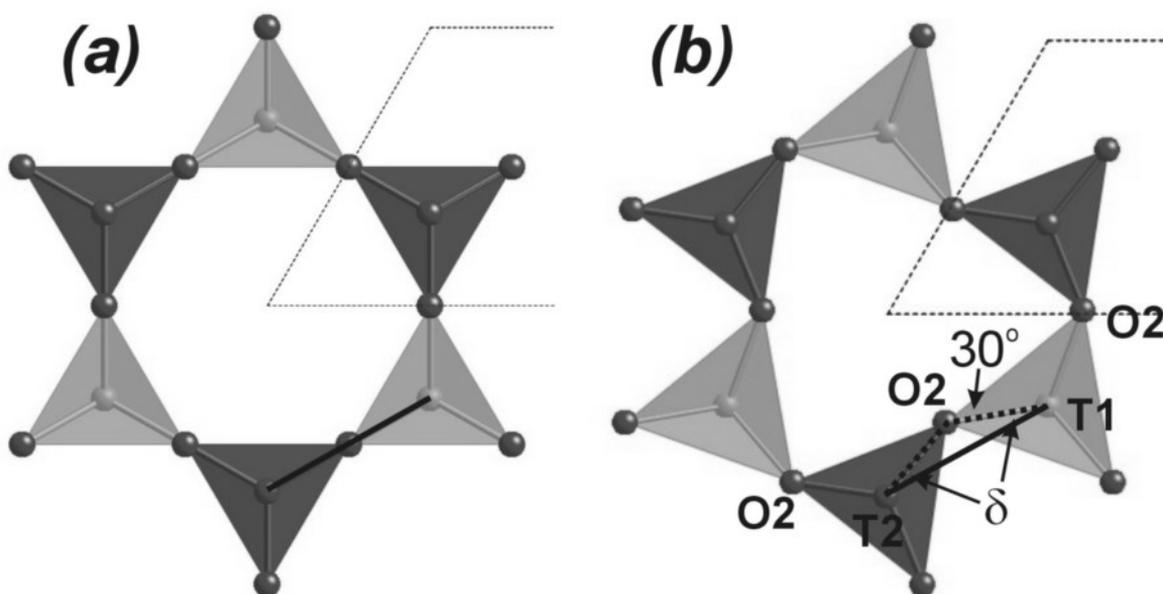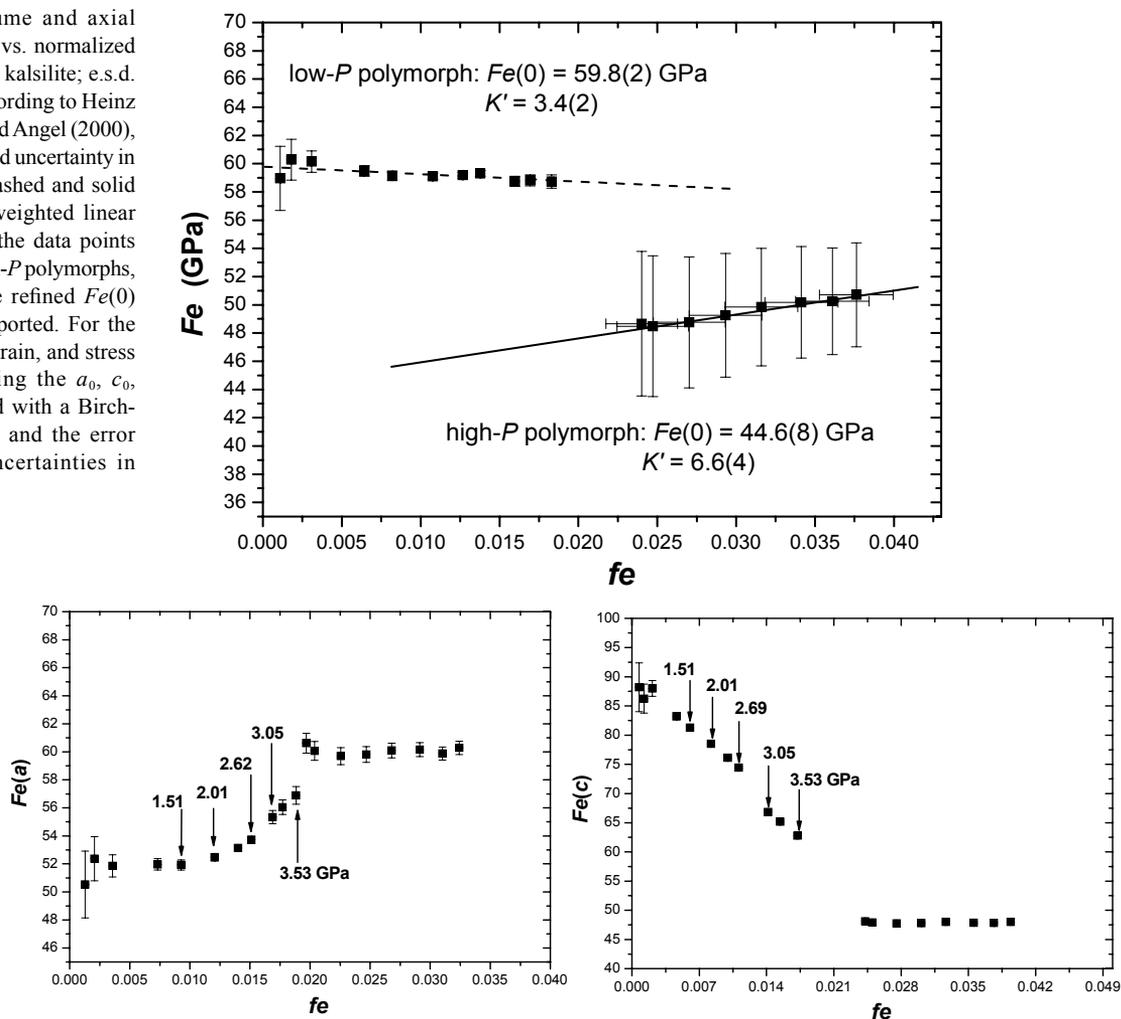

FIGURE 4. (**a**) A single 6mR of kalsilite viewed down [0001] with zero rotation and space group symmetry $P6_3mc$, equal to the topochemical symmetry. (**b**) The rotated 6mR in $P31c$ kalsilite at room conditions. The rotation angle is defined as the angle between the projections on to (0001) of the T1-T2 vector (solid line) and the T1-O2 and T2-O2 vectors (broken lines), and is: δ = |120 – (O2-O2-O2)|/2.
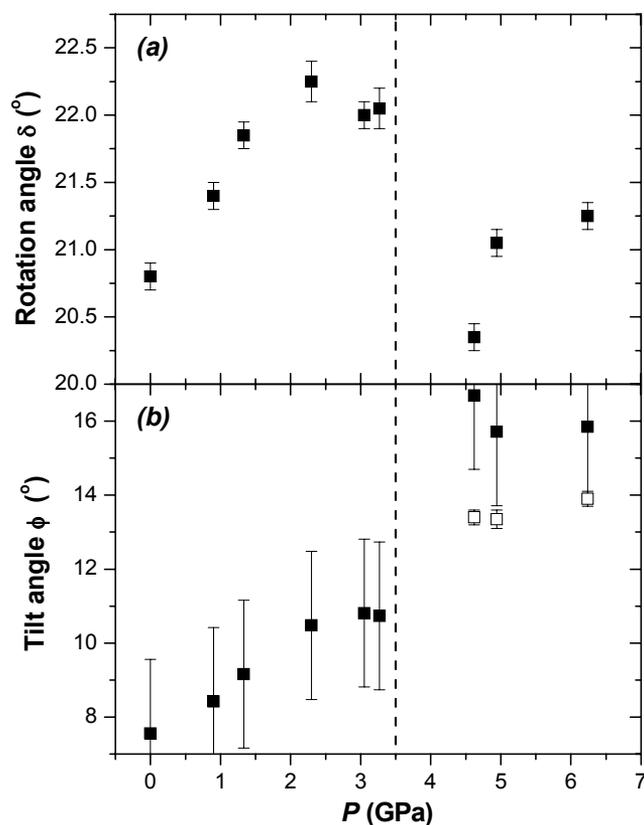
FIGURE 5. (**a**) Variation of the tetrahedral rotation angle δ, determined from the O2-O2-O2 angles. (**b**) Solid symbols are the variation of the tetrahedral tilt angle φ, determined from the T1-T2 distances assuming that the sum of the T1-O1 and T2-O1 distances is 3.35 Å. Open symbols are the tilt angles from the refinements of the split-site model for O1 in the high-pressure phase. The difference between these indicates that the T-O1 bond lengths have been compressed in the high-pressure phase. The vertical broken line indicates the approximate phase-transition pressure.

is therefore formally located at (1/3, 2/3, z), but the significantly anisotropic thermal displacement ellipsoid indicates an average over a true local structure with T1-O1-T2 angles less than 180°. If we consider normal Al-O and Si-O bond lengths at room conditions of 1.73 and 1.62 Å, respectively, we can estimate from the T1-T2 distance obtained from the data set collected in the DAC that the local value of the T1-O1-T2 angle is ~165° at 0.0001 GPa, corresponding to a tilt of the tetrahedra of φ = 180 − (T1-O1-T2)/2 ≈ 7.5°. Note that this estimate is greater than the 6° tilt angle estimated by Gatta et al. (2010a) from a full data set in air, but the difference is accounted for by the estimated uncertainties in the refined coordinates and cell parameters, which combine to produce an estimated uncertainty of ±2° in the T1-O1-T2 angle determined from the data sets collected in the DAC. An increase in the tilting of the tetrahedra will contribute to a decrease of both the a and c unit-cell parameters in proportion to cosφ.

0.0001 < P < 2.3 GPa

Over this pressure range, the most obvious change in the structure is the cooperative anti-rotation of the 6mR//(0001) tetrahedra (Fig. 5a) so as to increase the rotation angle δ and the distortion of the 6mR toward a more compressed "triangular" configuration, and to shorten the shorter O2-O2 distances across the ring. A decrease in the T1-T2 distance across O1 (Table 4) and an increase in the displacement parameters of both the O1 and O2 oxygen atoms (Table 3[1]) indicate that the tilts of the tetrahedra also increase (Fig. 5b). Both the increase in the tilt and the rotation contribute to the compression of directions within the (0001) plane, which is the a unit-cell parameter, but only the increase in tilt contributes to the compression of the c-axis, which explains why the [1000] direction is softer than [0001] (Fig. 3) and the c/a ratio initially increases with increasing pressure (Fig. 2). Within the experimental uncertainties, the z fractional coordinates of the two T sites do not change so the reduction in the c unit-cell parameter over this pressure range can be explained entirely by the increase in tilting of rigid tetrahedra to φ = 10.5°, and a T1-O1-T2 angle of ~159° at 2.30 GPa. In contrast, the combined effect of the rotation and tilting of rigid tetrahedra is significantly greater than that required to explain the reduction in the a unit-cell parameter, indicating that some additional structural relaxation, such as changes in the O-T-O angles, occurs within the tetrahedra.

~2.3 < P < ~3.5 GPa

Above 2.3 GPa, in the pre-transition interval, there is a continued compression of the unit-cell parameters, but no change in either the rotation angle of the tetrahedra or the tilts (Fig. 5). The fact that the T1-T2 distance across O1 remains constant (Table 4), means that all of the compression of [0001] must occur between the bases of the tetrahedra, across the O2 oxygen. There is a small contribution from compression of the T-O2 bonds (Fig. 6), but the changes in the O2-T1-O2 and O2-T2-O2 angles are in the opposite sense to one another (Table 4) and therefore cancel each other in their effect on the unit-cell axes. Therefore, the majority of the reduction in the c unit-cell parameter in this interval is accommodated simply by the "sliding" of the T1 and T2 tetrahedra past one another, a geometrical change that does not significantly change the T1-O2-T2 angle. A significant increase of the difference between the two torsion angles (i.e., O1-O2-O2′-O1$_a'$ and O1-O2-O2′-O1$_b'$, Fig. 1, Table 4) at ~2.3 < P < ~3.5 GPa supports such a hypothesis. Without a change in rotation or tilts of the tetrahedra, compression within the (0001) plane appears to be entirely accommodated by the shortening of the T-O2 bonds (Fig. 6).

However, this analysis in terms of a uniform structure does not take in to account the broadening of all but the 00l reflections in the pre-transition interval that indicates there is some inhomogeneity in the structure, and that the results of the structure refinements will be some form of average over whatever domains are formed. Similar line broadening was reported by Carpenter and Cellai (1996) for the $P6_3$-to-$P6_3mc$ transition at high-T, and they attributed it to the difference in the a-cell parameters of the different domains with different tetrahedral rotations. The same could be true here at high pressure, with some (0001) layers developing the larger rotations (and thus expanded a-cell parameter) of the HP structure. The fact that the 00l reflections remain sharp indicates that there is no disorder in the degree of tilting through the crystal, so the pre-transition interval appears to be a regime of disordered rotations but ordered tilts.
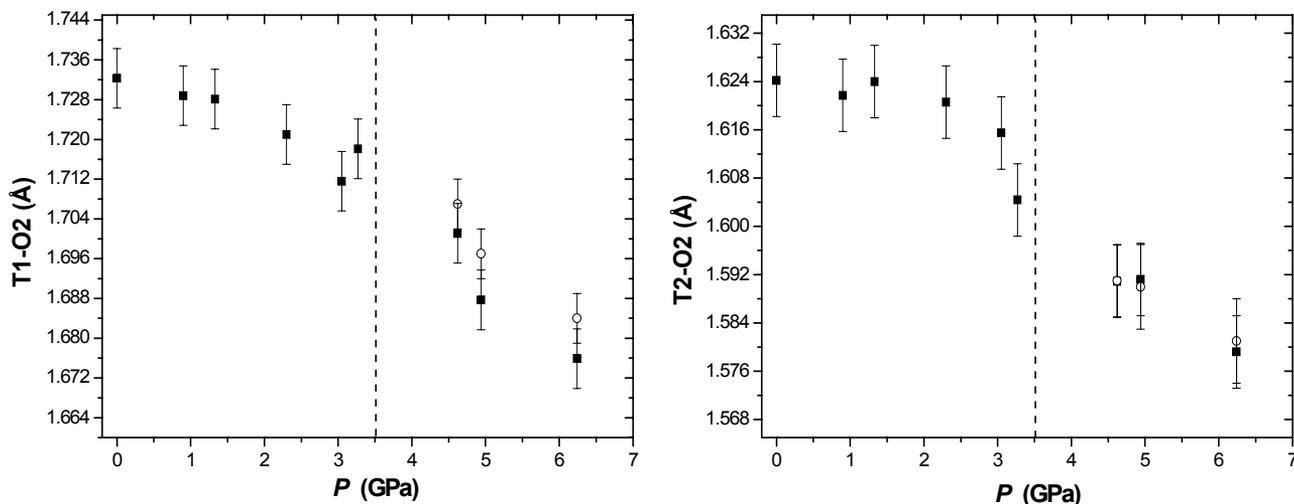
FIGURE 6. Evolution of the T1-O2 and T2-O2 bond distance with *P*. Open symbol = O1 site-split model. The vertical broken line indicates the approximate phase-transition pressure.

Phase transition

Structure refinements confirm that the high-pressure polymorph maintains the same *P*31*c* symmetry as the low-pressure polymorph. The crystal of the high-pressure polymorph is twinned by reticular merohedry with the {0001} twin plane, as observed for the low-pressure polymorph, and the refined volumes of the two twin components approach 50% each. The displacement parameters of both oxygen positions are significantly larger in the high-pressure phase than below the transition and therefore indicate that the tetrahedral tilts increase through the transition. This increase in tilts is sufficient to allow the stable refinement of a model with the O1 displaced from the threefold axis, to a general (*x*,*y*,*z*) position with site occupancy factor fixed to 1/3 (Table 3[1]), as has previously been refined for volcanic kalsilite (e.g., Perrotta and Smith 1965) and nepheline (e.g., Angel et al. 2008). The quality of the refinements with the O1-split model is superior (Table 1) to those with the O1 located on the triad, and the resulting tilts are 13.5° (Fig. 5) with a T-O-T angle of ~153°. Note that the value of the tilt obtained from these refinements is smaller than that predicted from the T1-T2 distance assuming that the T-O1 distances remain constant, and this provides independent confirmation that not only do the tilts increase but that the T-O bond lengths decrease at the transition.

Thus, the reduction in the *c* unit-cell parameter at the transition (Fig. 2) is the result of increased tilting. The transition is also accompanied by significant internal deformation of the tetrahedra as measured by the changes in the internal O2-T-O2 bond angles (Table 4), but these do not contribute to the volume reduction. The expansion in the (0001) plane arises from a reduction of the rotation angle of the tetrahedra back to approximately the value found at room pressure, which overcomes the combined effects of the increase in tilt and the compression of the T-O bond lengths.

~3.6 < *P* < ~6.2 GPa

Further compression of the high-pressure phase is significantly different from that in the low-pressure phase in that the tilts of the tetrahedra remain constant, so the compression of the *c*-axis is accommodated by compression of T-O2 bonds and the sliding of the tetrahedra past one another as seen in the pre-transition interval; this is also apparent from the evolution of the torsion angles (Table 4). The bond shortening also contributes to the compression of *a*, which is shortened by the re-initiation of increased rotations of the tetrahedra (Fig. 5a).

Structural evolution with pressure: Extra-framework content

The evolution of the tetrahedral framework of kalsilite with *P* defines the changes in the configuration of the extra-framework K-polyhedron. Within the stability field of the low-*P* polymorph (i.e., 0.0001–3.5 GPa), the increase in tetrahedral rotations causes the shorter K-O bond distances to compress faster than the longer ones, so that there is a slight increase in the anisotropy of the K-coordination (Table 4). Because the position of the O1 atom on the triad is an average position, no significance can be attributed to the values of K-O1 distances.

The first-order phase transition at ~3.5 GPa, with the drastic contraction along [0001] and the expansion on (0001), drives the structure toward a different channel configuration. At 4.62 GPa, the K-polyhedron is much more anisotropic, with three significantly shorter K-O2 bonds and three longer ones that differ by ~0.41 Å (Table 4). Further compression of the high-pressure phase leads to a faster compression of the longer K-O2 bonds so the anisotropy appears to become slightly less pronounced. A similar trend, toward a more anisotropic configuration, was observed for K-polyhedra in other classes of silicates at high pressure with the cation similarly coordinated by O atoms of double 6mRs of tetrahedra (Gatta et al. 2009, 2010b).

DISCUSSION AND CONCLUSIONS

This is the first experiment in which the behavior of kalsilite, with *P*31*c* symmetry, has been investigated at high pressure by means of single-crystal X-ray diffraction. Kalsilite experiences an iso-symmetric first-order phase transition at 3.5–3.6 GPa. The

phase transition is displacive in character and reversible, with no detectable hysteresis through the pressure intervals used in this study. The transition gives rise to a small expansion of the structure in the (0001) plane and a strong contraction along [0001]. The low-P polymorph is less compressible than the high-P one, a behavior already observed in other open-framework silicates belonging to the $Na_2O-K_2O-Al_2O_3-SiO_2$ system (Gatta et al. 2006, 2008). The elastic parameters reported by Fasshauer et al. (1998) for a synthetic $P6_3$ kalsilite on the basis of a Murnaghan EoS fit (Murnaghan 1937) to the P-V data (i.e., $K_{T0} \sim 58.6$ GPa, $K' \sim 0.1$) differ significantly from those obtained here, but it is not clear whether this difference represents a true difference between the polymorphs, or the effects of non-hydrostaticity in the experiments by Fasshauer et al. (1998).

Angel et al. (2008) and Gatta et al. (2010a) described the low-temperature structural evolution and thermo-elastic behavior of nepheline and kalsilite, respectively, showing that these two isotypic compounds do not respond to changes in temperature in the same way. Nepheline, in fact, has four independent tetrahedral sites (i.e., T1, T2, T3, and T4) that form a framework with two distinct 6mRs//(0001) in two different configurations (to produce large cavities for K and smaller cavities in which the smaller Na cations occupy ¾ of the channel sites). The more expanded of the two rings in nepheline, which has trigonal symmetry, is far less distorted than the rings in kalsilite. At room conditions, the diffraction pattern of $P6_3$ nepheline includes satellite reflections, and the structure refinement to the Bragg reflections shows that the O1 site is displaced from the triad at 2/3, 1/3, z (Gatta and Angel 2007; Angel et al. 2008). In their comparative analysis of the low-T behavior of kalsilite and nepheline, Gatta et al. (2010a) highlighted how the nature of the extra-framework population, through its bonding to the framework O atoms, can play a fundamental role in determining the structural response to temperature changes. The main deformation mechanism observed in kalsilite at low T reflects the mechanism observed here at high pressure for both the P-polymorphs: a cooperative anti-rotation of all tetrahedra of the 6mR//(0001) around [0001], as shown in Figure 5a.

At high pressure, Gatta and Angel (2007) observed a change in the compression mechanisms of nepheline arising from the changes in the O1 position associated with changes in the compression of the unit-cell axes and the unit-cell volume. The authors observed that, at 1.8 GPa, no significant intensity of the satellites occurred, the O1 site moved toward the triad, and thus the tilts of the T1 and T2 tetrahedra decreased. The presence of the subsidiary non-Bragg reflections was therefore related to the split of the O1 site. When the satellites disappear at pressures above 2 GPa, the O1 site is located on the triad (at 2/3, 1/3, z), leading to a straight T1-O1-T2 bond and thus the tilts of the T1 and T2 tetrahedra decreased to zero. Therefore, two main deformation mechanisms occur in nepheline: below 2 GPa, the structure responds to increased pressure by decreasing tilting of the T1 and T2 tetrahedra and increased tilting of the T3 and T4 tetrahedra, but above 2 GPa by tilting of the T3 and T4 tetrahedra alone. The change in the compressional mechanisms of nepheline does not lead to any phase transition. The elastic behavior was modeled by a fourth-order BM-EoS, with parameters: $V_0 = 723.57(4)$ Å³, $K_{T0} = 47.32(26)$ GPa, $K' = 2.77(24)$ and $K'' =$

0.758(79) GPa⁻¹, showing that nepheline is more compressible than the low-P kalsilite. The symmetry of (Si/Al "ordered") nepheline, the presence of four independent tetrahedral sites (i.e., T1, T2, T3, and T4) and, in particular, the nature of the extra-framework population (i.e., K, Na, Ca, and 20–25% site-vacancies, Gatta and Angel 2007; Angel et al. 2008) govern the higher degree of freedom of nepheline in response to T and P.

REFERENCES CITED

Abbott, R.N. Jr. (1984) KAlSiO₄ stuffed derivates of tridymite: Phase relationships. American Mineralogist, 69, 449–457.

Andou, Y. and Kawahara, A. (1982) The existence of high-low inversion point of kalsilite. Mineralogical Journal, 11, 72–77.

——— (1984) The refinement of the structure of synthetic kalsilite. Mineralogical Journal, 12, 153–161.

Angel, R.J. (2000) Equation of State. In R.M. Hazen and R.T. Downs, Eds., High-Temperature and High-Pressure Crystal Chemistry, vol. 41, p. 35–59. Reviews in Mineralogy and Geochemistry, Mineralogical Society of America and Geochemical Society, Chantilly, Virginia.

——— (2004) Absorption corrections for diamond-anvil pressure cells implemented in a software package Absorb-6.0. Journal of Applied Crystallography, 37, 486–492.

Angel, R.J. and Finger, L.W. (2011) SINGLE: a program to control single-crystal diffractometers. Journal of Applied Crystallography, 44, 247–251.

Angel, R.J., Allan, D.R., Miletich, R., and Finger, L.W. (1997) The use of quartz as an internal pressure standard in high-pressure crystallography. Journal of Applied Crystallography, 30, 461–466.

Angel, R.J., Downs, R.T., and Finger, L.W. (2000) High-Temperature–High-Pressure Diffractometry. In R.M. Hazen and R.T. Downs, Eds., High-Temperature and High-Pressure Crystal Chemistry, vol. 41, p. 559–596. Reviews in Mineralogy and Geochemistry, Mineralogical Society of America and Geochemical Society, Chantilly, Virginia.

Angel, R.J. Bujak, M., Zhao, J., Gatta, G.D., and Jacobsen, S.D. (2007) Static and ultrasonic observations on the effective hydrostatic limits of pressure media for high-pressure studies. Journal of Applied Crystallography, 40, 26–32.

Angel, J.R., Gatta, G.D., Boffa Ballaran, T., and Carpenter, M. (2008) The mechanism of coupling in the modulated structure of nepheline. Canadian Mineralogist, 46, 1465–1476.

Birch, F. (1947) Finite elastic strain of cubic crystal. Physical Review, 71, 809–824.

Badding, M.E., Marjanovic, S., Pinckney, L.R., and St. Julien, D.J. (2009) Glass-ceramic seals for use in solid oxide fuel cells. U.S. Patent Application: 20090075802.

Bogdanovicieni, I., Jankeviciute, A., Pinkas, J., Beganskiene, A., and Kareiva, A. (2008) Study of alumposilicate porcelain: sol–gel preparation, characterization and erosion evaluated by gravimetric method. Materials Research Bulletin, 43, 2998–3007.

Burnham, C.W. (1966) Computation of absorption corrections and the significance of end effects. American Mineralogist, 51, 159–167.

Capobianco, C.J. and Carpenter, M.A. (1989) Thermally induced changes in kalsilite. American Mineralogist, 74, 797–811.

Carpenter, M.A. and Cellai, D. (1996) Microstructures and high-temperature phase transitions in kalsilite. American Mineralogist, 81, 561–584.

Cellai, D., Bonazzi, P., and Carpenter, M. (1997) Natural kalsilite, KAlSiO₄, with $P31c$ symmetry: crystal structure and twinning. American Mineralogist, 82, 276–279.

Cellai, D., Gesing, T.M., Wruck, B., and Carpenter, M.A. (1999) X-ray study of the trigonal—hexagonal phase transition in metamorphic kalsilite. American Mineralogist, 84, 1950–1955.

Dollase, W.A. and Freeborn, W.P. (1977) The structure of KAlSiO₄ with $P6_3mc$ symmetry. American Mineralogist, 62, 336–340.

Fasshauer, D.W., Wunder, B., Chatterjee, N.D., and Höhne, G.W.H. (1998) Heat capacity of wadeite-type K₂Si₄O₉ and the pressure-induced stable decomposition of K-feldspar. Contributions to Mineralogy and Petrology, 131, 210–218.

Gatta, G.D. and Angel, R.J. (2007) Elastic behavior and pressure-induced structural evolution of nepheline: implications for the nature of the modulated superstructure. American Mineralogist, 92, 1446–1455.

Gatta, G.D., Nestola, F., and Boffa Ballaran, T. (2006) Elastic behavior, phase transition and pressure induced structural evolution of analcime. American

Mineralogist, 91, 568–578.

Gatta, G.D., Rotiroti, N., Boffa Ballaran, T., and Pavese, A. (2008) Leucite at high pressure: elastic behavior, phase stability and petrological implications. American Mineralogist, 93, 1588–1596.

Gatta, G.D., Rotiroti, N., Pavese, A., Lotti, P., and Curetti, N. (2009) Structural evolution of a 3T phengite mica up to 10 GPa: an in-situ single-crystal X-ray diffraction study. Zeitschrift für Kristallographie, 224, 302–310.

Gatta, G.D., Angel, R.J., and Carpenter, M.A. (2010a) Low-temperature behaviour of natural kalsilite with $P31c$ symmetry: an in-situ single-crystal X-ray diffraction study. American Mineralogist, 95, 1027–1034.

Gatta, G.D., Rotiroti, N., Pavese, A., Lotti, P., and Curetti, N. (2010b) Structural evolution of a $2M_1$ phengite mica up to 11 GPa: an in-situ single-crystal X-ray diffraction study. Physics and Chemistry of Minerals, 37, 581–591.

Gregorkiewitz, M. and Schäfer, H. (1980) The structure of $KAlSiO_4$-kaliophilite-O1: Application of the subgroup-supergroup relations to the quantitative space group determination of pseudosymmetric crystals. Sixth European Crystallographic meeting, Barcelona, July 28-August 1, Abstract, 155.

Gottardi, G. (1979) Topologic symmetry and real symmetry in framework silicates. Tschermaks Mineralogische und Petrographische Mitteilungen, 26, 39–50.

Heinz, D.L. and Jeanloz, R. (1984) The equation of state of the gold calibration standard. Journal of Applied Physics, 55, 885–893.

Henderson, C.M.B. and Taylor, D. (1982) The structural behavior of the nepheline family: (1) Sr and Ba aluminates (MAl_2O_4). Mineralogical Magazine, 45, 111–127.

——— (1988) The structural behavior of the nepheline family: (3) Thermal expansion of kalsilite. Mineralogical Magazine, 52, 708–711.

Hovis, G.L. and Roux, J. (1993) Thermodynamic mixing properties of nepheline-kalsilite crystalline solutions. American Journal of Science, 293, 1108–1127.

——— (1999) Thermodynamics of excess silicon in nepheline and kalsilite crystal-line solutions. European Journal of Mineralogy, 11, 815–827.

Hovis, G.L. and Crelling, J.A. (2000) The effects of excess silicon on immiscibility in the nepheline-kalsilite system. American Journal of Science, 300, 238–249.

Hovis, G.L., Crelling, J., Wattles, D., Dreibelbis, B., Dennison, A., Keohane, M., and Brennan, S. (2003) Thermal expansion of nepheline-kalsilite crystalline solutions. Mineralogical Magazine, 67, 535–546.

Hovis G. L., Person, E., Spooner, A., and Roux, J. (2006) Thermal expansion of highly silicic nepheline–kalsilite crystalline solutions: Mineralogical Magazine, 70, 383–396.

Hovis, G.L., Mott, A., and Roux, J. (2009) Thermodynamic, phase equilibrium, and crystal chemical behavior in the nepheline–kalsilite system. American Journal of Science, 309, 397–419.

Kawahara, A., Andou, Y., Marumo, F., and Okuno, M. (1987) The crystal structure of high temperature form of kalsilite ($KAlSiO_4$) at 950°C. Mineralogical Journal, 13, 260–270.

Kimura, R., Wakabayashi, J., Elangovan, S.P., Ogura, M., and Okubo, T. (2008) Nepheline from K_2CO_3/nanosized sodalite as a prospective candidate for diesel soot combustion. Journal of the American Ceramic Society, 130, 12844–12849.

King, H.E. and Finger, L.W. (1979) Diffracted beam crystal centering and its application to high-pressure crystallography. Journal of Applied Crystallography, 12, 374–378.

Klyne, W. and Prelog, V. (1960) Description of steric relationships across single bonds. Experientia, 16, 521–523.

Liu, L. (1987) High-pressure phase transitions of potassium aluminosilicates with an emphasis on leucite. Contributions to Mineralogy and Petrology, 95, 1–3.

Mao, H.K., Xu, J., and Bell, P.M. (1986) Calibration of the ruby pressure gauge to 800 kbar under quasi-hydrostatic conditions. Journal of Geophysical Research, 91, 4673–4676.

Merlino, S. (1984) Feldspathoids: their average and real structures. In W.L. Brown, Ed., Feldspars and Feldspathoids. Structures, properties and occurrences, vol. 137, p. 435–470. NATO Advanced Study Institutes, Series C: Mathematical and Physical Sciences, Dordrecht.

Miletich, R., Allan, D.R., and Kuhs, W.F. (2000) High-pressure single-crystal techniques. In R.M. Hazen and R.T. Downs, Eds., High-Temperature and High-Pressure Crystal Chemistry, vol. 41, p. 445–519. Reviews in Mineral-ogy and Geochemistry, Mineralogical Society of America and Geochemical Society, Chantilly, Virginia

Murnaghan, F.D. (1937) Finite deformations of an elastic solid. American Journal of Mathematics, 49, 235–260.

Oxford Diffraction (2009) Oxford Diffraction Ltd., Xcalibur CCD system, CrysAlis Software system.

Perrotta, A.J. and Smith, J.V. (1965) The crystal structure of kalsilite, $KAlSiO_4$. Mineralogical Magazine, 35, 588–595.

Sahama, T.G. (1962a) Perthite-like exsolution in the nepheline–kalsilite system. Norsk Geologisk Tidsskrift, 43, 168–179.

——— (1962b) Order–disorder in natural nepheline solid solutions. Journal of Petrology, 65–81.

Sandiford, M. and Santosh, M. (1991) A granulite facies kalsilite-leucite-hibonite association from Punalur, Southern India. Mineralogy and Petrology, 43, 225–236.

Sheldrick, G.M. (2008) A short history of SHELX. Acta Crystallograhica, A64, 112–122.

Tuttle, O.F. and Smith, J.V. (1958) The nepheline-kalsilite system: II. Phase rela-tions. American Journal of Science, 256, 571–589.

Wen, G., Yan, Z., Smith, M., Zhang, P., and Wen, B. (2010) Kalsilite based hetero-geneous catalyst for biodiesel production. Fuel, 89, 2163–2165.

Wilson, A.J.C. and Prince, E., Eds. (1999) International Tables for X-ray Crystal-lography, Volume C: Mathematical, physical and chemical tables, 2nd ed., Kluwer Academic, Dordrecht, Netherlands.

Xu, H. and Veblen, D.R. (1996) Superstructures and domain structures in natural and synthetic kalsilite. American Mineralogist, 81, 1360–1370.

Zhang, Y., Ming, L.V., Dongdan, C., and Jianqing, W. (2007) Leucite crystallization kinetics with kalsilite as a transition phase. Materials Letters, 61, 2978–2981.